# Uptake of Formic Acid on Thin Ice Films and on Ice Doped with Nitric Acid between 195 and 211 K

**ARTICLE** *in* CHEMPHYSCHEM · DECEMBER 2010

Impact Factor: 3.42 · DOI: 10.1002/cphc.201000434 · Source: PubMed



**5 AUTHORS**, INCLUDING:

Manolis N Romanias
Ecole des Mines de Douai
**25** PUBLICATIONS **99** CITATIONS
SEE PROFILE

Vassileios Papadimitriou
University of Crete
**30** PUBLICATIONS **378** CITATIONS
SEE PROFILE

Panos Papagiannakopoulos
University of Crete
**66** PUBLICATIONS **659** CITATIONS
SEE PROFILE

CHEMPHYSCHEM

DOI: 10.1002/cphc.201000434

# Uptake of Formic Acid on Thin Ice Films and on Ice Doped with Nitric Acid between 195 and 211 K

Manolis N. Romanias, Antonia G. Zogka, Vassileios G. Stefanopoulos, Vassileios C. Papadimitriou, and Panos Papagiannakopoulos*[a]

The adsorption of formic acid on thin ice films and on ice doped with nitric acid (1.96, 7.69 and 53.8 wt%) is studied as a function of temperature $T = 195$–$211$ K and gas concentration $(0.33–10.6)\times10^{11}$ molecule cm$^{-3}$. Experiments are performed in a Knudsen flow reactor coupled with a quadrupole mass spectrometer. The initial uptake coefficients $\gamma$ are strongly and inversely dependent on the ice temperature. Initial uptake is determined at low surface coverages and ranges from $(0.65–3.78)\times10^{-3}$. The adsorption uptake of formic acid on pure ice films and on ice lightly doped with $HNO_3$ is a reversible process, and the adsorption isotherms exhibit Langmuir behaviour. $N_{max}(1)$ is $(2.94\pm0.67)\times10^{14}$ molecule cm$^{-2}$, in good agreement with previous measurements. The temperature dependence of $K_{Lin}$ is very well represented by the expression: $K_{Lin}(1) = (1.43\pm0.32)\times10^{-8}\exp[(4720\pm520)/T]$ cm$^3$ molecule$^{-1}$; the quoted uncertainty is at the 95% level of confidence and includes systematic uncertainties. Formic acid uptakes on ice films highly doped with $HNO_3$ (53.8 wt%) are two orders of magnitude higher than those measured on pure ice films and irreversible, thus indicating the formation of a supercooled liquid layer on the ice films upon which dissolution of formic acid occurs. Finally, the atmospheric lifetime of formic acid due to heterogeneous loss on cirrus cloud ice particles and the removal of formic acid by adsorption are estimated under conditions related to the upper troposphere.

## 1. Introduction

The heterogeneous chemistry of halogenated and nitrated trace gases on stratospheric ice particles has been an important scientific issue in the last decade, due to its significance to stratospheric ozone depletion.[1] Several experimental studies have shown that these molecules interact strongly with pure or doped ($HNO_3$, $H_2SO_4$) ice particles and therefore they may initiate new heterogeneous processes in polar stratospheric clouds.[2] However, less attention has been given to the heterogeneous interaction of hydrocarbons, including oxygenated volatile organic compounds (OVOCs), on ice surfaces, although such species are in considerable mixing ratios in the upper troposphere (UT) and may play an important role in tropospheric chemistry.[1] Carboxylic acids are among the most abundant OVOCs with mixing ratios up to 792 ppt, which are generated via several homogeneous and heterogeneous photochemical processes or directly emitted by vegetation and biomass burning.[3] They are considered as potential sources of $HO_x$ radicals and therefore they may also participate in the photochemical cycle of tropospheric ozone. Furthermore, carboxylic acids are polar, weak and quite soluble organic acids, which are formed in the atmospheric and aqueous environment via oxidation of hydrocarbons.[4]

Moreover, nitric acid traces have been detected in the mid and upper troposphere with mixing ratios of 0.1–2 ppb,[5] and in the lower stratosphere (LS) as crystalline nitric acid trihydrate (NAT).[6] In addition, condensed-phase $HNO_3$ has been observed in cirrus clouds in the UT at levels higher than 0.8 ppbv, and the mean percentage of total $HNO_3$ condensed on cirrus cloud particles was 16%.[7] Although the partitioning of nitric acid gas in ice cloud particles is not well understood, it appears that nitric acid molecules are trapped during the ice particle growth in the UT/LS region, which results in ice particles doped with $HNO_3$ or NAT particles.[6,7] It is therefore important to investigate the adsorption of carboxylic acids on ice films doped with $HNO_3$.

In the literature, there are only a few experimental studies that have investigated the interaction of small oxygenated gaseous molecules with pure ice films or with ice films doped with $HNO_3$ at low temperatures.[1,8–11] In particular, the heterogeneous interaction of formic acid with pure ice surfaces has been studied by Hessberg et al.[12] in the temperature range 187–221 K, and more recently by Symington et al.[13] in the temperature range 208–228 K, both using the coated-wall laminar flow tube (CWLFT) technique. However, there are no experimental data for the adsorption of formic acid on ice surfaces doped with $HNO_3$, which are encountered in the UT/LS region of the atmosphere. There are also no experimental data for the initial uptake coefficients $\gamma$ of formic acid on pure ice films or on ice films doped with $HNO_3$.

[a] Dr. M. N. Romanias, A. G. Zogka, Dr. V. G. Stefanopoulos, Dr. V. C. Papadimitriou, Prof. Dr. P. Papagiannakopoulos
Laboratory of Photochemistry and Kinetics
Department of Chemistry, University of Crete
71003 Heraklion, Crete (Greece)
Fax: (+30) 2810-545-001
E-mail: panosp@chemistry.uoc.gr

Supporting information for this article is available on the WWW under http://dx.doi.org/10.1002/cphc.201000434.

The aim of the present study was to measure the initial uptake coefficient $\gamma$ of formic acid on thin ice films and on ice films doped with various percentages of $HNO_3$ at several gas concentrations and ice temperatures between 195 and 211 K. The adsorption enthalpy and entropy was also determined by examining the temperature dependence of $\gamma$. Moreover, the surface coverage $N_s$ of formic acid on thin ice films and on films doped with $HNO_3$ was determined in the same low-temperature range, and the saturation surface coverage $N_{max}$ was derived by employing the Langmuir adsorption model. The temperature dependence of the partition constant $K_{Lin}$ ($K_{Lin} = K_{Lang} \times N_{max}$) for the different ice films was also determined. Finally, the importance and implications of the above kinetic and thermodynamic parameters in the heterogeneous chemistry of formic acids in the atmosphere are discussed.

## Experimental Section

The uptake measurements of formic acid on thin ice and $HNO_3$/ice films were performed using the continuous-flow molecular system of very low pressure reactor (VLPR) coupled with a quadrupole mass spectrometer (QMS). The VLPR/QMS technique has been employed in the past to measure the absolute rate coefficients for gas-phase reactions between Cl atoms and hydrocarbons of atmospheric interest.[14,15] It consisted of three main units: a) a gas preparation glass vacuum line that included storage bulbs and buffer volumes in series with resistance capillaries to create steady molecular flows of reactants, b) a Knudsen reactor designed to measure uptakes of gas molecules on ice surfaces, and c) a two-stage stainless steel vacuum system equipped with a QMS (QMG 422) to detect volatile reactants and products. The mass spectrometric signals were modulated by a tuning fork chopper, amplified by a lock-in amplifier (SR8300, DSP), and finally converted to a digital form via an analogue-to-digital data acquisition card (Advantech PCI-1710 L) and stored in a PC for subsequent analysis.

Knudsen Reactor: The Knudsen reactor, total volume $V = 535\ cm^3$, was made out of glass and had three gas inlets on the top and one outlet on the side, which was connected to the two-stage vacuum system via variable orifices (1–5 mm). A schematic diagram is presented in Figure 1. The reactor had a metallic plunger sliding perpendicularly in the centre of the reactor via an O-ring setting, in the lower part of which was a round Teflon disc for isolating or exposing the ice surface to the molecular flow. The bottom part of the reactor consisted of a copper flange that was adapted to the reactor via an outer Teflon ring, and both were vacuum-sealed with Viton O-rings. The upper part of the copper flange was a round flat surface (area = 12.56 $cm^2$) upon which ice films were deposited, and the lower part (surface 50 $cm^3$) was immersed in a methanol bath, continuously cooled by a refrigerator unit (Haake, EK90). The methanol bath was kept inside a double-wall vacuum Dewar and its temperature was regulated and adjusted within $\pm 0.1$ K by using a heating resistance controlled by a thermostat (Shimaden, SR91). The temperature was continuously monitored with a Pt-100 thermocouple sensor. The internal reactor surface was coated with a thin Teflon layer (DuPont, FEP 121a) to inhibit wall reactions. Finally, the reactor was also heated up to 323 K to control the gas-phase temperature and avoid water condensation on the walls.

It is well known that formic acid molecules undergo dimerization under certain pressure and temperature conditions,[16,17] and therefore the presence of dimers in our experiments should be examined. In the Knudsen flow reactor technique the kinetic energy of gas molecules prior to adsorption may take several values depending on the wall temperature (in our case it was 323 K), whereas in the CWLFT technique gas molecules take only the value of the low-temperature wall. It is estimated that at room temperature the dimerization reaction HC(O)OH↔HC(O)OH···HC(O)OH reaches equilibrium within 20 ms.[12] In our flow system, the residence time of HC(O)OH molecules in the glass line and the Knudsen reactor ($t_r$ = 2.2 s) was much longer than 20 ms, and therefore this reaction was at equilibrium. Considering that the partial pressure of formic acid inside the Knudsen reactor was in the range $0.1–5 \times 10^{-5}$ Torr and the temperature was 323 K, the mole fraction of formic acid dimers is estimated to be negligible in our system, and thus no corrections for formic acid dimerization were made in the analysis of experimental data. In addition, uptake coverages were determined by following both *m/z* 45 and 46 mass peaks, and the obtained values were identical, which indicated that both mass peaks originated from a single species (HC(O)OH monomer) with no measurable contribution from dimer fragmentation at *m/z* 46.

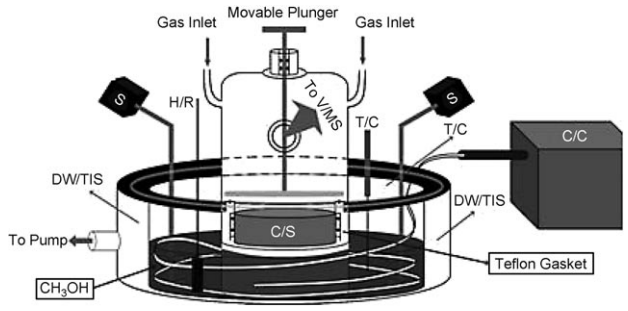


**Figure 1.** Simplified schematic diagram of a Knudsen reactor in which the major components are presented: a) formic acid and water vapour inlets, and the movable plunger in the upper part; b) the external Teflon and the inner copper flanges (C/S) connected via Viton O-rings in the bottom part; and c) the side outlet connecting the reactor with the quadrupole mass spectrometer chamber. The ice films are grown on the upper round part of the copper flange (C/S), while the bottom part is cooled by a methanol bath cryostated with a refrigerator unit. Abbreviations used in the figure: C/S: Cooper Substrate, C/C: Cooling Circulating Unit, S: Electrical Stirrer, V/MS: Vacuum/Mass Spectrometry System, T/C: Thermocouple, DW/TIS: Double Walled Thermally Isolated System, H/R: Heating Resistance, TIC: Thermal Isolating Cover.

Another complication in our Knudsen reaction experiments may originate from possible dissociation and ionization of "hot" HC(O)OH molecules upon striking the ice surface. Several experimental studies have shown that the adsorption of formic acid molecules on ice surfaces under similar temperature and pressure conditions does not lead to any detectable dissociation.[18–21] However, in the case when some dissociation of formic acid molecules occurs on the ice surface it should produce formate, which subsequently may either diffuse into the ice bulk or abstract a proton and further desorbed in the gas phase as formic acid. To investigate the likelihood of the latter process, we performed uptake experiments of formic acid and HCl on $D_2O$ ice surfaces. Although the H/D exchange process in and/or on the surface was clearly present in the interaction of HCl (strong acid) with the ice surface by observing DCl, no deuterated formic acid was observed in product analysis. The first process was also excluded, since the uptake signals were fully reversible, which suggested very limited or no diffusion of formic acid or products into the ice bulk. Most importantly, it should be pointed out that employment of the dissocia-

  

tive Langmuir model[22] did not fit our experimental data on pure ice films or ice doped with $HNO_3$. On the contrary, our experimental data fit the Langmuir-type model very satisfactorily, which suggests that the dissociation process does not occur to an appreciable degree under our experimental conditions.

Thin Ice Film Preparation: The water ice films were prepared by passing a steady molecular flow of $H_2O$ vapour ($\approx 2.6\times 10^{17}$ molecule $s^{-1}$) over a copper substrate at 206 K for a period of about 20 min. The ice formation process was monitored by measuring the molecular flow of $H_2O$ ($m/e=18$) at three consecutive positions of the plunger: a) the plunger down, keeping the cold surface isolated; b) the plunger up, exposing the surface to the water flow; and c) the plunger down, again isolating the surface from the water flow (see the Supporting Information, Figure S1). By lifting the plunger up, $H_2O$ molecules were deposited slowly on the copper substrate to form thin water ice films. This preparation procedure was efficient and reproducible, and is considered to produce thin ice films without significant cracks and porosity, which consist of ice particles with a hexagonal structure ($I_h$) and size approximately 5 μm.[23–25] Although previous surface vibrational spectroscopic studies have indicated that the disordering and melting of the ice surface initiates at around 200 K,[26] recent molecular-beam studies have lowered this limit to 180 K.[27] Upon completion of the above ice growth process the substrate temperature was adjusted gradually to the desired temperature. Subsequently, a continuous steady flow of water vapour was applied over the developed ice films, which was adjusted until no change in water partial pressure occurred upon opening and closing the plunger. This water flow was always present in our uptake measurements to maintain a constant ice film thickness. The ice film temperatures were determined both experimentally and by using the relation between water vapour pressure and temperature.[28–30] Even though the difference between the two methods was less than 1%, the second method was selected to record the ice film temperatures, by interpolating the experimental values given by Marti and Mauersberger.[30]

The steady-state concentration of $H_2O$ was about $2.8\times 10^{14}$ molecule $cm^{-3}$. The total number of $H_2O$ molecules adsorbed on the cold substrate in a given time interval was determined by converting the mass spectral signals to $H_2O$ flow ($F_{H2O}=I_{H2O}/a_{H2O}$ molecule $s^{-1}$) and integrating the surface area under the $F_{H2O}$ (see Figure S1 in the Supporting Information). The thickness of the ice films was estimated by considering the hexagonal structure of ice; hence a unit cell consisted of four $H_2O$ molecules. The number of adsorbed $H_2O$ molecules was about $2\times 10^{20}$ molecules, which corresponds to $\approx 5\times 10^{19}$ unit cells of ice. Since each unit cell has a volume of $1.31\times 10^{-22}$ $cm^3$, the calculated ice volume was $V_{ice}=6.55\times 10^{-3}$ $cm^3$. Therefore, the film thickness was determined to be ice volume/ice area $=6.55\times 10^{-3}$ $cm^3/12.56$ $cm^2=5.2$ μm. Assuming that each monolayer of ice contains $1\times 10^{15}$ molecule $cm^{-2}$, the solid ice films consisted of approximately 16000 monolayers (MLs), with a building-up rate of 13 ML $s^{-1}$. This procedure of thin ice film growth was reproducible, since the total number of water molecules adsorbed under the same ice preparation conditions was the same within 5%. The majority of the uptake experiments were performed with solid ice films 5–6 μm in thickness; however, certain experiments were performed with ice films of thickness up to 20 μm that produced identical results, thus providing a strong indication that within the timescale of our experiments the process of HC(O)OH uptake on pure ice films was dominated by monolayer adsorption.

The ice films doped with $HNO_3$ were prepared by flowing simultaneously $H_2O$ molecules and $HNO_3$/He mixtures over the copper surface at 206 K for 30–60 min, through separate inlets. The steady-state concentrations of $H_2O$ and $HNO_3$ molecules were $(0.5–2)\times 10^{14}$ and $(1–10)\times 10^{13}$ molecule $cm^{-3}$, respectively. The initial sticking coefficient $\gamma$ of $HNO_3$ on the copper surface at 206 K was zero in the absence of water flow, while during co-adsorption of $HNO_3$ and $H_2O$ molecules the derived $\gamma$ values were $(1.5\pm 0.06)\times 10^{-2}$ and $(1.15\pm 0.04)\times 10^{-2}$, respectively. The initial uptake coefficient of $HNO_3$ on ice films was also measured at 203 K and was found to be $(6.0\pm 0.5)\times 10^{-3}$, with steady-state concentrations of $HNO_3$ circa $1.5\times 10^{-5}$ Torr. Although there is a reasonable agreement of our value with the literature values, $\gamma(HNO_3)=7\times 10^{-3}$ at 209 K[31] and $(3.3\pm 0.6)\times 10^{-2}$ at 214 K,[32] considering the quoted uncertainties they cannot be directly compared since the temperature and $HNO_3$ concentration regimes were different in those experiments. In addition, the $\gamma(H_2O)$ values at 206 K were independent of the absence or presence of $HNO_3$ molecules, which suggested that the ice growth on the copper surface was initiated by a water condensation process. Therefore, $\gamma(H_2O)$ should depend only on the flow rates and partial pressures of the gas-phase molecules, and consequently on the substrate temperature, and not on their chemical composition. Thus, our $\gamma(H_2O)$ values were consistently lower than the previously reported values of 0.04–0.15 derived in the temperature range 180–220 K.[33] As far as the co-adsorption process is concerned, it appears that $H_2O$ molecules, with higher flow rates, are initially adsorbed efficiently on the copper surface forming solid ice deposits, upon which $HNO_3$ molecules are subsequently co-adsorbed with almost similar rates building relatively homogeneous multilayer structures. The co-adsorbed numbers of $H_2O$ and $HNO_3$ molecules on the cold surface were derived by integrating the surface area under the $I_{H2O}$ ($m/z$ 18) and $I_{HNO3}$ ($m/z$ 46) mass spectrometric signals, respectively, and converting them to flows over the time window of the process. It was estimated that the ice films contained 1.96, 7.69 and 53.8 wt% of $HNO_3$, by flowing $HNO_3$/He mixtures of 7.4, 8.5 and 11.2%, respectively. A recent molecular-beam and light-scattering study has reported that the co-adsorption of gaseous $HNO_3$ and $H_2O$ molecules on copper surfaces at 170 K resulted in fast ice film growth, which is attributed to the stability and chemistry of the involved sub-monolayer structures.[34] According to the phase diagram of the $HNO_3/H_2O$ mixture, 1.96–53.8 wt% for temperatures below 230 K, the binary systems are in the solid-phase domain consisting of ice and β-NAT (nitric acid trihydrate, $HNO_3{\cdot}3H_2O$).[35] Recent FTIR measurements have shown that the co-deposition of $H_2O$ and $HNO_3$ molecules at surfaces of $T=190$ K lead to the formation of β-NATs.[25,36]

The morphology of water ice films and ice doped with $HNO_3$, deposited from the vapour on several substrates under low temperature and pressure conditions, has been investigated by environmental scanning electron microscopy (ESEM).[23,37,38] In the temperature range 180–200 K, the thin ice films were composed of ice particles with hexagonal structure and sizes between 2 and 8 μm (average size ca. 5 μm). By increasing the temperature to 215 K, the ice particles become larger, slowly lose their hexagonal structure, and consequently their boundaries gradually disappear. At even higher temperatures the sintering and consolidation continues and the ice particles are not distinguishable any more. The ice films doped with $HNO_3$ (containing 39–82 wt% $HNO_3$) at 200 K were also composed of water ice and NAT particles with hexagonal structure and roughly uniform size of around 5 μm. Hence, under our experimental conditions ($T=195–211$ K) it is safe to assume that the pure ice films consist of ice particles with hexagonal structure and average size about 5 μm, while the ice films doped with

  

$HNO_3$ consist of water ice particles and several NAT particles (depending on the degree of nitration) with similar hexagonal structure and size.

Kinetic Uptake Measurements: The steady-state concentration of stable molecules in the Knudsen reactor is given by the expression [Eq. (1)]:

$$[M] = F_M/(k_{esc,M}V_{cell}) = I_M/(\alpha_M V_{cell} k_{esc,M}) \quad (1)$$

where $I_M$ is the mass peak intensity, $\alpha_M$ is the mass calibration factor and $F_M$ is the reactant flow rate (in molecule $s^{-1}$). The latter parameters were determined by separate calibration experiments.[14] The escape rate coefficient $k_{esc,M}$ of all species is given by the expression $k_{esc,M} = A_{sc} \times (T/m)^{1/2}\ s^{-1}$, where $A_{esc} = 0.16\ s^{-1}$ for a 2 mm orifice ($T$ = temperature and $m$ = molecular mass of M). Hence, the residence times of $H_2O$ and HC(O)OH in the Knudsen reactor were 1.4 and 2.2 s, respectively. Formic acid flows and concentrations were determined by measuring the mass peak intensities of the parent and fragment peaks at $m/z$ 46 and 45, respectively. The mass spectral intensities were taken at 70 eV, and were measured with an uncertainty of $\approx$1% at the 95% level of confidence.

A typical uptake profile of formic acid on pure ice films at 195 K is presented in Figure 2a. The initial uptake coefficient and surface coverage of formic acid on pure ice films were determined by monitoring the mass peak intensities at $m/z$ 45 and/or 46 as a function of time upon exposing the ice surface to the formic acid flow. The formic acid uptakes on ice films doped with $HNO_3$ were obtained by monitoring the mass peak at $m/z$ 45 to avoid a contribution from $HNO_3$.

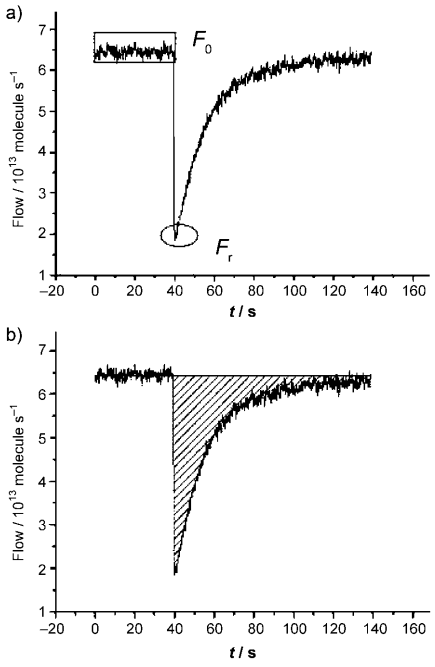


**Figure 2.** a) Typical adsorption profile of formic acid molecules on pure ice films at 195 K, used to determine initial uptake based on Equation (2). b) The number of formic acid molecules adsorbed on the ice films (molecule $cm^{-2}$) is given by integrating the area under this adsorption profile. $F_0$ and $F_r$ correspond to molecular flows isolating and exposing the ice surface to the gas environment, respectively.

In a Knudsen reactor, the initial uptake coefficient ($\gamma$) of a gas molecule M on a surface area $A_s$ is given by the expression [Eq. (2)]:

$$\gamma(t) = \frac{k_{upt}}{\omega} = \frac{4V_R k_{esc,M}}{u_M A_s} \frac{(F_{0,M} - F_{r,M})}{F_{r,M}} \quad (2)$$

where $k_{upt} = k_{esc}[(F_{0,M} - F_{r,M})/F_{r,M}] = k_{esc,M}[(I_{0,M} - I_{r,M})/I_{r,M}]$, and $\omega = u_M A_s/4V_R$, $F_{r,M}$, $F_{0,M}$, $I_{r,M}$ and $I_{0,M}$ are the molecular flows and mass spectral intensities of the gas molecule exposing and isolating the ice surface from the gas environment, respectively, and $\omega$ is the collision frequency of gases with the ice surface ($u_M = 1.46 \times 10^4 (T/m)^{1/2}$).

The initial uptake coefficient of formic acid on thin ice films was determined at 195 K using two escape apertures 2 and 3 mm ($k_{esc,HC(O)OH} = 0.43$ and $1.03\ s^{-1}$, respectively), and the obtained values were $(3.78 \pm 0.26) \times 10^{-3}$ and $(3.92 \pm 0.31) \times 10^{-3}$, respectively; the quoted uncertainties are the $2\sigma$ precision [Eq. (2)]. This finding clearly indicates that $\gamma$ measurements were independent of $k_{esc}$ within experimental error, and that Equation (2) is valid. The area under the uptake profile of formic acid on ice films (Figure 2b) provides the total number of formic acid molecules adsorbed by the surface, and corresponds to the surface coverage $N_s$ (molecules $cm^{-2}$).

Chemicals: The chemicals/gases used in this study were commercially available with stated purity or synthesized. Formic acid (Sigma–Aldrich, 96%) was purified by fractional distillation and by repeated freeze–pump–thaw cycles. Then, it was further diluted in He (Linde, 99.7%) in 0.72 and 0.62% mixtures. Nitric acid was synthesized via the reaction of sulphuric acid with potassium nitrate and was cryo-trapped at 77 K to form solid $HNO_3$. Subsequently, $HNO_3$ was evaporated and diluted in He to form 7.4, 8.5 and 11.2% mixtures, which were stored in dark glass bulbs to avoid decomposition to $NO_2$. The purity of these mixtures was measured prior to each experiment by mass spectrometry ($I_{46}/I_{30} \approx 1.68$) and FTIR spectroscopy. Nanopure $H_2O$ that was previously degassed by several freezing/melting cycles was used for the preparation of the ice films.

## 2. Results and Discussion

### 2.1. Uptake Experiments on Pure Ice Surfaces

The initial uptake coefficient $\gamma$ of formic acid on pure ice films was measured as a function of gas concentration in the range $(0.6–9) \times 10^{11}$ molecules $cm^{-3}$ at several ice temperatures between 195 and 208 K. The $\gamma$ values were determined to be in the range $(0.65–3.78) \times 10^{-3}$, and are listed in Table 1. To our knowledge, this is the first study reporting the initial uptake coefficients of formic acid on pure ice films. Since there are no previous experimental studies, our values may be compared with the $\gamma$ values reported for other atmospheric trace gases in the same temperature range, which are given in Table 2. Our $\gamma$ values for formic acid on ice are lower than those for OH, HCl, $HNO_3$, $CH_3OH$, $N_2O_5$ and $CH_3C(O)CH_3$ gases, similar to those for HONO, and higher or much higher than those for $NO_3$, $NO_x$ and $O_3$.

The initial uptake coefficient $\gamma$ was found to decrease with increasing temperature, as shown in Table 1. The initial drop of the uptake signal, until it reaches a minimum value within 1–2 s, is dominated by the adsorption of formic acid molecules

  

**Table 1.** Initial uptake coefficient $\gamma$ for formic acid adsorption on pure ice films and on ice doped with 1.96, 7.69 and 53.8 wt% $HNO_3$ at several temperatures. The adsorption enthalpy and entropy of formic acid on pure ice films are also given. The quoted uncertainties represent the precision and are given at the 95% level of confidence.

| $T$ [K] | [HCO(O)H][a] | Experiments | $\gamma \times 10^3$ |
|---|---|---|---|
| Pure ice | | | |
| 195 | 1.00–4.08 | 6 | $3.78 \pm 0.26$ |
| 198 | 0.60–2.31 | 5 | $2.10 \pm 0.15$ |
| 201 | 1.08–3.76 | 5 | $1.48 \pm 0.10$ |
| 203 | 1.01–3.09 | 11 | $1.12 \pm 0.08$ |
| 208 | 1.14–4.92 | 7 | $0.65 \pm 0.05$ |
| $\Delta H_{ads} = -(45.0 \pm 5.3)$ kJ mol$^{-1}$, $\Delta S_{ads} = -(278 \pm 52)$ J mol$^{-1}$ K$^{-1}$ | | | |
| Ice doped with 1.96 wt% $HNO_3$ | | | |
| 195 | 1.80–7.00 | 8 | $1.42 \pm 0.10$ |
| 201 | 1.81–7.12 | 10 | $1.30 \pm 0.091$ |
| 203 | 2.92–7.85 | 7 | $1.22 \pm 0.08$ |
| Ice doped with 7.69 wt% $HNO_3$ | | | |
| 195 | 1.42–2.1 | 2 | $4.62 \pm 0.32$ |
| 201 | 1.13–4.45 | 6 | $2.54 \pm 0.18$ |
| 203 | 0.91–11.80 | 17 | $0.96 \pm 0.07$ |
| Ice doped with 53.8 wt% $HNO_3$ | | | |
| 195 | 2.88–5.49 | 10 | $>28.40$ |
| 203 | 2.19–4.91 | 10 | $>13.90$ |

[a] [HC(O)OH] in $10^{11}$ molecule cm$^{-3}$.

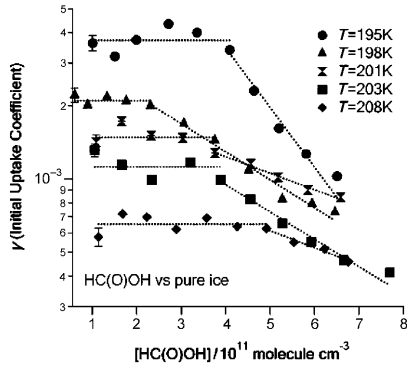


**Figure 3.** Initial uptake coefficient $\gamma$ (solid symbols) of formic acid molecules on pure ice films as a function of gas-phase concentration at 195, 198, 201, 203 and 208 K. At low formic acid concentrations, $\gamma$ remains constant (linear fits), while at high concentrations $\gamma$ decreases exponentially, as seen by the exponential fit of the data. Error bars reflect the $2\sigma$ precision of the measured $\gamma$ values ($\approx 7\%$).

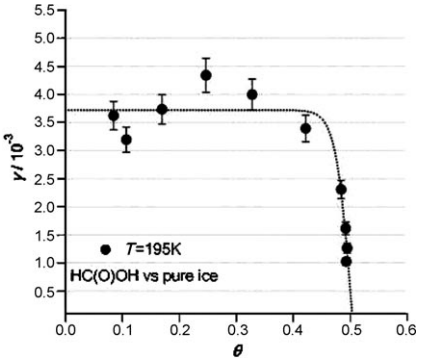


**Figure 4.** Initial uptake coefficient $\gamma$ of formic acid molecules on pure ice films as a function of surface coverage $\theta$ at 195 K. Error bars reflect the $2\sigma$ precision of the measured $\gamma$ values. The dotted line is a sigmoid fit used for presentation purposes to illustrate the dependence of $\gamma$ on surface coverage $\theta$.

on the ice surface; adsorbate–adsorbate interactions are negligible. At the same time desorption of formic acid from the ice surface starts to compete, approaching equilibrium at later times. At lower ice temperatures the adsorption becomes faster and desorption slower, and therefore $\gamma$ values are higher. At low formic acid concentrations $\gamma$ is independent of concentration, which indicates low ice surface coverages. However, at formic acid partial pressures higher than $1.5 \times 10^{-5}$ Torr the $\gamma$ value decreased exponentially with concentration, as shown in Figure 3. In addition, the $\gamma$ value showed a strong dependence on surface coverage $\theta$ for values higher than 0.5, as presented in Figure 4. This behaviour suggests that at high formic acid concentrations the surface coverage becomes substantial, thus restricting the incoming gas-phase molecules from approaching the active sites on the ice surface. It also indicates that a possible interaction between gas-phase and adsorbed formic acid molecules is expected to be very weak and will not contribute to the initial uptake of HC(O)OH on the ice surface.

The overall uptake process may be interpreted by using the precursor adsorption model.[39] According to this model the incoming gas molecule $M_{(g)}$ does not undergo direct adsorption on the surface, but is initially accommodated on the surface with a rate $\alpha k_t$, producing a steady-state surface concentra-

**Table 2.** Initial uptake coefficient $\gamma(\times 10^3)$ for several atmospheric trace gases on pure ice films as a function of temperature. The temperature range [K] is given in parentheses.

| Trace gas | Initial uptake coefficient ($\gamma \times 10^3$) | | | | | |
|---|---|---|---|---|---|---|
| OH | 100 (205–230)[48] | | | | | |
| HCl | $70 \pm 30$ (205)[49] | | | | | |
| $HNO_3$ | $170 \pm 50$ (200)[50] | $90 \pm 30$ (209)[50] | | 7 (209)[9] | | 3 (220)[9] |
| $CH_3OH$ | $>20$ (198)[8] | | | | | |
| $N_2O_5$ | $20 \pm 2$ (200)[51] | | | | | |
| $CH_3C(O)CH_3$ | 6 (193–218)[52] | | | | | |
| HONO | 1 (180–200)[53] | | | 0.64 (200)[54] | | |
| $NO_3$ | $<1$ (170–200)[55] | | | | | |
| NOx | $<5 \times 10^{-3}$ (193–243)[56] | | | | | |
| $O_3$ | $<1 \times 10^{-3}$ (195–262)[57] | | | | | |
| HC(O)OH[a] | $3.78 \pm 0.43$ (195) | $2.10 \pm 0.1$ (198) | $1.48 \pm 0.16$ (201) | $1.12 \pm 0.14$ (203) | $1.07 \pm 0.21$ (206) | $0.65 \pm 0.05$ (208) |

[a] This work.

  

tion $[M]_{(p)}$, until it encounters an empty site on which it is physically adsorbed with a rate $k_a$ or desorbed with a rate $k_d$. The overall interaction scheme for HC(O)OH molecules is given by [Eq. (3)]:

$$[HC(O)OH]_{(g)} \underset{k_d}{\overset{\alpha k_t}{\longleftrightarrow}} [HC(O)OH]_{(p)} \xrightarrow{k_a} [HC(O)OH]_{(ads)} \quad (3)$$

where $\alpha$ is the mass accommodation coefficient, which is unity for thermal velocities, and $k_t$ is the rate coefficient for trapping of the molecule in the precursor state p. Thus, the initial uptake coefficient $\gamma$ is given by the expression [Eq. (4)]:

$$\gamma = \frac{\text{adsorption rate}}{\text{collision rate}} = \frac{k_a[HC(O)OH]_{(p)}}{\alpha k_t[HC(O)OH]_{(g)}} \quad (4)$$

Assuming a steady state for $[HC(O)OH]_{(p)}$ in Equation (3), it results in [Eq. (5)]:

$$[HC(O)OH]_p = \frac{\alpha k_t[HC(O)OH]_{(g)}}{k_d + k_a} \quad (5)$$

Combining Equations (4) and (5) and $\alpha = 1$, the relation between the initial uptake coefficient, $k_a$ and $k_d$ gives [Eq. (6)]:

$$\gamma = \frac{1}{1 + (k_d/k_a)} \quad (6)$$

However, the ratio of rate constants can be expressed in terms of the observed Gibbs free energy barrier of the transition state towards adsorption relative to the gas phase [Eq. (7)]:[40]

$$\frac{k_a}{k_d} = \exp(-\Delta G^{\ddagger}_{ads}/RT) \quad (7)$$

Combining Equations (6) and (7), and substituting $\Delta G^{\ddagger}_{ads} = \Delta H_{ads} + T\Delta S_{ads}$ results in [Eq. (8)]:

$$\ln\left(\frac{\gamma}{1-\gamma}\right) = \left(\frac{-\Delta G^{\ddagger}_{ads}}{RT}\right) = \frac{-\Delta H_{ads}}{RT} + \frac{\Delta S_{ads}}{R} \quad (8)$$

Therefore, the adsorption enthalpy and entropy can be derived by plotting $\ln[\gamma/(1-\gamma)]$ versus $1000/T$. For low formic acid concentrations, where $\gamma$ was measured to be independent of HC(O)OH concentration, this plot is shown in Figure 5, which provides the values $\Delta H_{ads} = -(45.0 \pm 5.3)$ kJ mol$^{-1}$ and $\Delta S_{ads} = -(278 \pm 52)$ J mol$^{-1}$ K$^{-1}$; the uncertainties reflect the $2\sigma$ precision of the least-squares fits.

The surface coverage ($N_s$) of formic acid on pure ice films was measured as a function of gas concentration in the range $(0.33–7.7) \times 10^{11}$ molecules cm$^{-3}$ and at several temperatures between 195 and 208 K. The adsorption isotherms of formic acid on pure ice films at several temperatures are presented in Figure 6. Each point represents the average of several uptake measurements (at least four independent measurements at each HC(O)OH concentration) that were taken on fresh ice films to ensure repeatability and reproducibility, and increase the accuracy of our measurements. The surface coverage data were analysed by employing the Langmuir and Brunauer–Emmett–Teller (BET) isotherm models.

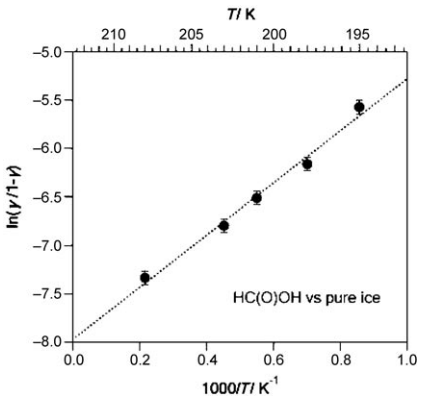


**Figure 5.** Plot of $\ln[\gamma/(1-\gamma)]$ versus $1000/T$, according to Equation (6), at formic acid concentration regions where $\gamma$ was independent of surface coverage. Error bars reflect the $2\sigma$ precision of $\ln[\gamma/(1-\gamma)]$ values, while the dotted line is the least-squares fit to the data.

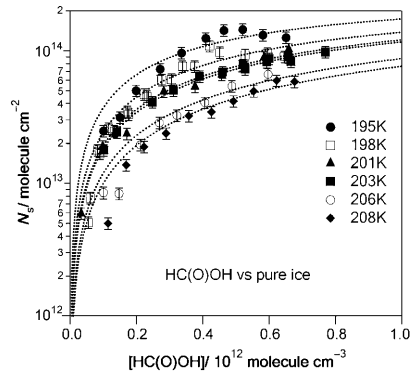


**Figure 6.** Adsorption isotherms of formic acid on pure ice films at 195, 198, 201, 203, 206 and 208 K. The dotted lines correspond to the Langmuir model fitting given by Equation (7). Error bars represent the $2\sigma$ precision on $N_s$ determination.

The basic assumption of the Langmuir adsorption model is that the uptake of a gas molecule on a solid surface cannot proceed beyond monolayer coverage, and the number of formic acid molecules adsorbed per surface area depends on the gas-phase concentration, according to Equation (9):

$$\theta = \frac{N_s}{N_{max}} = \frac{K_{Lang}[HC(O)OH]}{1 + K_{Lang}[HC(O)OH]} \quad (9)$$

where $\theta$ is the surface coverage of formic acid molecules on the ice surface, $N_s$ is the number of formic acid molecules adsorbed (in molecules cm$^{-2}$), $N_{max}$ is the monolayer saturation surface coverage (in molecules cm$^{-2}$) and $K_{Lang}$ (in cm$^3$ molecule$^{-1}$) is the Langmuir equilibrium constant, which describes the partitioning between the gas phase and gas adsorbed on the surface molecules. The Langmuir-type adsorption model was employed to fit our experimental data and its

  

fit was very good, as shown in Figure 6. This finding clearly indicates that the experimental isotherms are satisfactorily described in terms of the Langmuir model, with the additional assumptions that all adsorption sites are equivalent and the interactions between adsorbed molecules are negligible. The $N_{max}$ value was derived by fitting the experimental data to Equation (8) at $T=203$ K, the value obtained being $N_{max}(1)=(2.94\pm0.67)\times10^{14}$ molecules cm$^{-2}$. The $N_{max}$ value is best derived at low temperatures, where the surface coverage is the largest for given gas concentrations. However, $N_{max}$ depends on the number and reactivity of adsorption sites and is expected to be independent of temperature. Thus, the $N_{max}$ value was determined at 203 K, for which more experimental data and wider range of formic acid concentrations were available, thus achieving a more accurate fit to the Langmuir model.

**Table 3.** Saturation surface coverage ($N_{max}$) and adsorption enthalpy ($\Delta H_{ads}$) for formic acid adsorption on pure ice films and on ice doped with 1.96, 7.69 and 53.8 wt% $HNO_3$. Partitioning constants $K_{Lang}$ and $K_{Lin}$ at different temperatures. The estimated error uncertainties were approximately 10% ($2\sigma$).

| T [K] | [HCOOH][a] | $N_{max}$[b] | $K_{Lang}$[c] | $K_{Lin}$[d] | $-\Delta H_{ads}$[e] |
|---|---|---|---|---|---|
| Pure ice | | | | | |
| 195 | 1.00–6.51 | | $17.14\pm2.48$ | $503.92\pm73.38$ | |
| 198 | 0.55–6.46 | | $10.10\pm1.10$ | $296.94\pm32.55$ | |
| 201 | 0.33–6.59 | $2.94\pm0.67$ | $7.19\pm0.56$ | $211.38\pm16.39$ | (39.24±4.32) |
| 203 | 1.01–7.70 | | $6.37\pm0.28$ | $187.28\pm8.28$ | |
| 206 | 1.00–5.97 | | $4.36\pm0.46$ | $128.18\pm13.49$ | |
| 208 | 1.14–6.76 | | $3.57\pm0.24$ | $104.96\pm7.27$ | |
| $K_{Lin}(1)=(1.43\pm0.32)\times10^{-8}\exp[(4720\pm520)/T]$ | | | | | |
| Ice doped with 1.96 wt% $HNO_3$ | | | | | |
| 195 | 0.85–11.93 | | $17.06\pm1.6$ | $670.46\pm63.11$ | |
| 201 | 0.55–8.72 | $3.93\pm0.34$ | $7.34\pm1.10$ | $288.46\pm43.39$ | (49.81±8.46) |
| 203 | 2.13–9.24 | | $4.93\pm0.50$ | $193.75\pm19.72$ | |
| $K_{Lin}(2)=(3.08\pm0.24)\times10^{-11}\exp[(5991\pm1018)/T]$ | | | | | |
| Ice doped with 7.69 wt% $HNO_3$ | | | | | |
| 195 | 0.75–7.16 | | $29.45\pm3.56$ | $2035\pm247$ | |
| 201 | 0.60–6.86 | $6.91\pm0.76$ | $6.27\pm0.80$ | $433.26\pm55.6$ | (87.38±6.94) |
| 203 | 0.62–11.8 | | $3.44\pm0.42$ | $237.70\pm29.20$ | |
| $K_{Lin}(3)=(8.43\pm1.80)\times10^{-21}\exp[(10500\pm835)/T]$ | | | | | |
| Ice doped with 53.8 wt% $HNO_3$ | | | | | |
| 195 | 0.82–10.85 | | $0.45\pm0.02$ | $1845\pm82$ | |
| 203 | 2.02–13.40 | $410\pm40$ | $0.42\pm0.04$ | $1722\pm165$ | (2.52±0.38) |
| 211 | 2.94–16.09 | | $0.40\pm0.04$ | $1640\pm165$ | |
| $K_{Lin}(4)=(387\pm85)\ \exp[(303\pm46)/T]$ | | | | | |

[a] [HC(O)OH] in $10^{11}$ molecule cm$^{-3}$. [b] $N_{max}$ in $10^{14}$ molecule cm$^{-2}$. [c] $K_{Lang}$ in $10^{-13}$ cm$^3$ molecule$^{-1}$. [d] $K_{Lin}=N_{max}xK_{Lang}$ in cm. [e] $\Delta H_{ads}$ in kJ mol$^{-1}$.

Once the $N_{max}$ value is determined, the $K_{Lang}$ value can be derived at different temperatures using the expression [Eq. (10)]:

$$\frac{\theta}{1-\theta}=K_{Lang}(T)[HC(O)OH]_{gas} \quad (10)$$

which is a rearrangement of Equation (9). The plots of $\theta/(1-\theta)$ versus [HC(O)OH] at various temperatures (see the Supporting Information, Figure S2), and the obtained $K_{Lang}$ and $K_{Lin}(=K_{Lang}\times N_{max})$ values are given in Table 3. The $N_{max}(1)$ value for formic acid is in good agreement with previous experimental values of $(2.2\pm0.5)\times10^{14}$ and $(2.13\pm0.26)\times10^{14}$ molecules cm$^{-2}$ reported by Hessberg et al.[12] and Symington et al.,[13] respectively. The Symington et al.[13] value was taken at 208 K, since they report an inverse temperature dependence of $N_{max}$. Furthermore, this value is in good agreement with the values for acetic acid, a molecule with similar chemical behaviour: $(2.4\pm0.6)\times10^{14}$, $(2.6\pm0.6)\times10^{14}$ and $(2.34\pm0.90)\times10^{14}$ molecules cm$^{-2}$ reported by Hessberg et al.,[12] Sokolov et al. ($T=222$–$245$ K),[41] and Symington et al.[13] ($T=208$ K), respectively. Our $K_{Lang}$ values at 198 and 208 K are smaller by factors of about 50 and 30, respectively, than those reported by Hessberg et al.,[12] and smaller by a factor of 13 than the value of Symington et al.[13] at 208 K. This discrepancy may be due, to some extent, not only to the large uncertainties in the literature values (22–40%), but also to the uncertainty of $\Delta S_{ads}$ values (see below). Therefore, our $K_{Lin}$ values were also lower by a factor of 37 and 13 than the values of Hessberg et al.,[12] and by a factor of 8 compared with the value of Symington et al.[13]. The temperature dependence of the Langmuir equilibrium constant is given by the Van't Hoff expression [Eq. (11)]:

$$K_{Lang}=A\exp[-(\Delta H_{ads}/RT)] \quad (11)$$

where $A$ is the pre-exponential factor and $R$ is the ideal gas constant. The plot of $K_{Lang}$ versus $1000/T$ provides the adsorption enthalpy of formic acid on pure ice films (see the Supporting Information, Figure S3). Therefore, the temperature dependence of $K_{Lang}$ determined in this work is given by Equation (12):

$$K_{Lang}(1)=(4.88\pm1.08)\times10^{-23}\exp[(4720\pm520)/T] \quad (12)$$

and the expression of $K_{Lin}$, based on the $N_{max}$ determined in the present work ($K_{Lin}=K_{Lang}\times N_{max}$) is [Eq. (13)]:

$$K_{Lin}(1)=(1.43\pm0.32)\times10^{-8}\exp[(4720\pm520)/T] \quad (13)$$

The quoted uncertainties on $\Delta H_{ads}$ reflect the $2\sigma$ precision of the least-squares fit of $\ln K$ versus $1000/T$, while the error limit on $A$ is related to the intercept of the fit based on the expression $dA=A\times d(\ln A)$. All the systematic uncertainties have been included in the pre-exponential factor quadratically $[(\Delta A)^2=(dA)^2+(\text{systematic})^2]$. Therefore, $\Delta H_{ads}=$

  

$-(39.24\pm4.32)$ kJ mol$^{-1}$, which overlaps with the previously derived value $-(45.0\pm5.3)$ kJ mol$^{-1}$ using the $\gamma$ values, taking into account the precision of our measurements. Finally, Equation (12) is in excellent agreement with the expression $K_{Lin}(1) = (1.50\pm0.20)\times10^{-8}\exp[(5130\pm400)/T]$[13] reported by Symington et al.,[13] although their $K_{Lang}$ and $K_{Lin}$ values are higher by a factor of about 10 relative to our values mainly due to the small observed differences in exponential ($\approx$1.1 times) factors.

The BET isotherm model was also employed to fit our experimental data to compare the $N_{max}$ values obtained by both isotherm models, as well as to explore the likelihood of multilayer formation on the ice surface. According to the BET isotherm, which is valid for high surface coverage, the maximum number of adsorbed molecules in a monolayer $N_{max}$ is given by the expression [Eq. (14)]:

$$Y = \frac{[HCOOH]}{N_s([HCOOH]_0 - [HCOOH])} = \frac{1}{N_{max}C} + \frac{C-1}{N_{max}C}\frac{[HCOOH]}{[HCOOH]_0} \quad (14)$$

where $C$ is the dimensionless BET constant and $[HC(O)OH]_0$ is the saturation gas-phase concentration, which was found to be $3.79\times10^{13}$ molecule cm$^{-3}$ at 203 K by using the Antoine equation.[42] The plot of $Y$ versus $[HCOOH]/[HCOOH]_0$ provides the ratios $(C-1)/N_{max}C$ and $1/N_{max}C$, and therefore the values of $N_{max}$ and $C$ (see the Supporting Information, Figure S4). The derived values were $N_{max} = (2.16\pm0.67)\times10^{14}$ molecule cm$^{-2}$ and $C = 27.9$ at 203 K; the quoted uncertainty reflects the $2\sigma$ precision of least-squares analysis. This $N_{max}$ value is in good agreement with the value derived using the Langmuir isotherm model, which suggests that the uptake of formic acid on pure ice surfaces was limited to monolayer coverage.

The $\Delta H_{ads}$ value using the precursor adsorption model is in excellent agreement with the values (Langmuir analysis) $-(44\pm3)$ and $-(51\pm4)$ kJ mol$^{-1}$ reported by Symington et al.[13] and Hessberg et al.,[12] respectively, as well as with the value determined in this work using Langmuir analysis [$K_{Lin}(T)$], $-(39.24\pm4.32)$ kJ mol$^{-1}$. Although the $\Delta S_{ads}$ derived by this work based on Langmuir analysis, $-(12\pm11)$ J mol$^{-1}$ K$^{-1}$, is in reasonable agreement with the corresponding values of $-(17\pm15)$ and $-(43\pm19)$ J mol$^{-1}$ K$^{-1}$ reported by Symington et al.[13] and Hessberg et al.,[12] respectively, the $\Delta S_{ads}$ value determined by employing the precursor adsorption model is much higher. It is worth mentioning that Hessberg et al.[12] considered the determination of $\Delta S_{ads}$ based on Van't Hoff plots unreliable due to the large extrapolation involved in the narrow-temperature-regime analysis performed.

In general, the adsorption enthalpy is expected to show very little dependence on the surface coverage, since the binding energy of an adsorbed molecule with the surface depends primarily on the affinity of the ice surface. In contrast, the adsorption entropy is expected to exhibit a much stronger dependence on the surface coverage, since the steric interactions between incoming gas molecules and adsorbed molecules become more pronounced at higher surface coverages, due to the need for the incoming molecule to adjust its orientation to undergo adsorption.

The precursor adsorption model is mainly valid at low surface coverages, when the interactions between adsorbed molecules are negligible. In our study the thermodynamic parameters were determined using the $\gamma$ values, which were found to be independent of concentration at low surface coverages (see Figures 3 and 4). Therefore, the validity of the precursor model is secured and the obtained enthalpy and entropy values are more reliable. The Langmuir model is also valid at low surface coverages, but at increased $\theta$, where adsorbate–adsorbate interactions become more pronounced, the Langmuir model imposes limitations. Thus, the thermodynamic parameters reported in this work were obtained by employing the precursor adsorption model, and the values derived using the Langmuir analysis are presented for comparison purposes.

### 2.2. Uptake Experiments on Ice Films Doped with $HNO_3$

Uptake experiments of formic acid molecules on ice films doped with $HNO_3$ (1.96, 7.69 and 53.8 wt%) were performed as a function of concentration at several temperatures between 195 and 211 K. Typical comparative uptake profiles of formic acid on pure ice films and on ice doped with $HNO_3$ at 195 K and $[HC(O)OH] = 7\times10^{11}$ molecule cm$^{-3}$ are presented in Figure 7. The uptake profiles become significantly higher by increasing the degree of ice film nitration, and become completely irreversible for ice films doped with 53.8 wt% $HNO_3$. This behaviour is consistent with the previously described nature and structure of the ice films upon nitration. At low nitration (1.96 and 7.68 wt%), the thin ice films are expected to contain mainly water ice particles and a few NAT particles,[23,37,38] which increase slightly the reactivity and possibly the number of surface sites, and consequently the corresponding adsorption probability. At high nitration (53.8 wt%), the ice films are expected to contain mainly NAT particles,[23,37,38] which increase substantially the reactivity of the surface sites, thus resulting in much higher and irreversible uptakes.

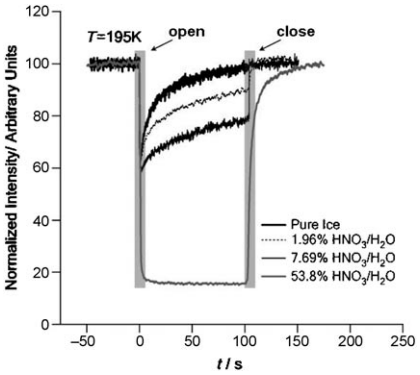


**Figure 7.** Uptake profiles for a constant formic acid concentration ($\approx7\times10^{11}$ molecules cm$^{-3}$) on pure ice films and on ice doped with $HNO_3$ at 195 K. "Open" and "close" correspond to the up and down positions of the plunger, respectively.

  

Furthermore, the above behaviour may be explained in terms of a multilayer adsorption or the appearance of a supercooled liquid layer on the ice films that induces dissolution and diffusion processes. However, our experimental isotherms tend to level off at high formic acid concentrations (Figure 8),

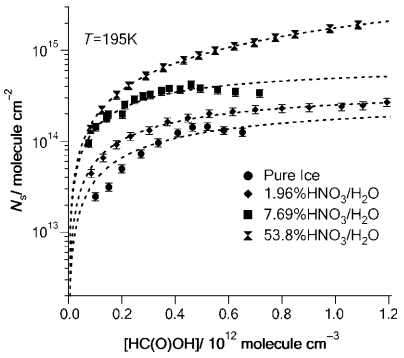


**Figure 8.** Adsorption isotherms of formic acid on pure ice films and on ice doped with 1.96, 7.69 and 53.8 wt% $HNO_3$ at 195 K. The surface coverage $N_s$ (molecule cm$^{-2}$) is derived by integration of the adsorption profile. The dashed lines correspond to the Langmuir model fitting given by Equation (7), while the error bars represent the $2\sigma$ precision on $N_s$ determination.

which is not consistent with the BET adsorption model for multilayer coverages. On the contrary, the formation of a supercooled liquid solution during preparation of ice films doped with $HNO_3$ has been observed in previous studies,[43,44] in the temperature regime 200–210 K depending on the degree of nitration. Indeed, such supercooled liquid layer formation is consistent with the observation of higher uptakes upon increasing the amount of nitric acid, and eventually these uptakes become irreversible at high nitration (53.8 wt%).

The initial uptake coefficient $\gamma$ of formic acid on ice films doped with 1.96, 7.68 and 53.8 wt% $HNO_3$ was measured as a function of concentration at 195, 201 and 203 K. The $\gamma$ values obtained are given in Table 1. In the case of ice films doped with 1.96 and 7.68 wt% $HNO_3$, the $\gamma$ values were constant at low formic acid concentrations and were strongly diminished at high concentrations and large surface coverages, like in pure ice films. For ice films highly doped with $HNO_3$ (53.8 wt% $HNO_3$), the reported $\gamma$ values represent a lower limit, since the $\gamma$ values were decreasing at increased formic acid concentrations. The $\gamma$ values on ice films with low degree of nitration (Table 1) were smaller than or similar to that obtained on pure ice films. This may be due the limited change in the nature of the ice particles in the ice films within the initial adsorption period. On the contrary, for ice films highly doped with $HNO_3$ (53.8 wt% $HNO_3$), the $\gamma$ values were much higher than those obtained for pure ice films, and depended on the formic acid concentration. This behaviour is consistent with the above-described formation of a supercooled solution layer upon nitration.

Although the uptake process of formic acid on pure ice films was completed within 100 s, on the ice films doped with $HNO_3$ the uptake was extended to several minutes or was never completed (53.8 wt% doping), as presented in Figure 7. Moreover, the $N_s$ value was substantially increased by increasing the degree of ice film nitration. This is clear evidence that diffusion processes into the ice bulk are initiated upon nitration of the ice films. In particular, for ice films highly doped with $HNO_3$ (53.8 wt% $HNO_3$) the $N_s$ values were two orders of magnitude higher than for pure ice films, for the first 100 s. For comparison reasons, the $N_s$ value for the doped ice films was taken by integrating over the first 100 s, since the 2/3 criterion is fulfilled (see below). Within this time period the adsorption and desorption processes for pure ice films and doped films of low nitration are in the steady state and any further change is negligible. The Langmuir-type adsorption model fits these experimental data rather well, as shown in Figure 8 at 195 K. It is worth noting that although the primary assumptions of the Langmuir model are violated in adsorption processes on reactive surfaces, it may be used in cases where the uptake signal recovery is higher than 2/3 of its initial value,[22,45,46] which was valid in our lightly doped ice film experiments. The $K_{Lang}$ values at different temperatures are given in Table 3. Figure 8 also shows the adsorption isotherms of formic acid on pure ice films and doped with $HNO_3$ at 195 K, as well as the corresponding Langmuir fits. The $N_{max}$ values for ice films doped with $HNO_3$ (1.96 (2), 7.69 (3) and 53.8 (4) wt%) were determined at 195 K, and were found to be $N_{max}(2) = (3.93 \pm 0.34) \times 10^{14}$, $N_{max}(3) = (6.91 \pm 0.76) \times 10^{14}$ and $N_{max}(4) = (410 \pm 40) \times 10^{14}$ molecule cm$^{-2}$. The high $N_{max}$ values, especially for the ice films highly doped with $HNO_3$, is consistent with the formation of a supercooled liquid layer that initiates dissolution of formic acid molecules into this interface layer and probably diffusion into the ice bulk.

Furthermore, the temperature dependence of the partitioning constant $K_{Lin}$ was derived at different degrees of nitration. The obtained expressions are:

$K_{Lin}(2) = (3.08 \pm 0.24) \times 10^{-11} \exp[(5991 \pm 1018)/T]$,

$K_{Lin}(3) = (8.43 \pm 1.80) \times 10^{-21} \exp[(10\,500 \pm 835)/T]$ and

$K_{Lin}(4) = (387 \pm 85) \exp[(303 \pm 46)/T]$ cm$^3$ molecule$^{-1}$.

The plots of the above expressions are shown in Figure 9. It appears that the adsorption process becomes more exothermic ($\Delta H_{ads}$ more negative) upon increasing the degree of ice

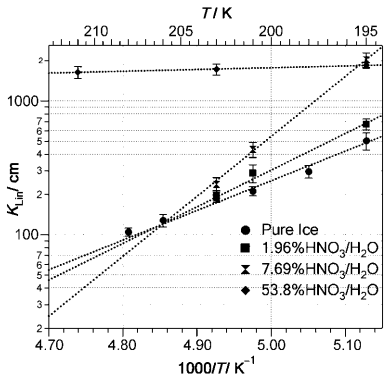


**Figure 9.** Plots of $K_{Lin}$ versus 1000/$T$ for pure ice films and for ice doped with 1.96, 7.69 and 53.8 wt% $HNO_3$. Dashed lines are the fits to the data based on the expression $K_{Lin} = A\exp(-\Delta H/RT)$. Error bars reflect the precision of $K_{Lin}$ at the 95% level of confidence.

  

film nitration in the range of 0–7.69 wt%, which suggests that $HNO_3$ molecules strengthen the interaction between formic acid and ice surface molecules. On the contrary, the pre-exponential factors decrease drastically (several orders of magnitude) at higher ice film nitration, which indicates that $HNO_3$ molecules reduce the entropy change in the interaction of formic acid with ice surface molecules, most likely due to orientation restrictions (adsorbate–adsorbate interactions) and/or possible electrolytic dissociation or protonation of HC(O)OH on NAT particles. For highly enriched ice films (53.8 wt%), the uptake was irreversible and $K_{Lin}$ was almost independent of temperature. This is clear evidence that the adsorption and dissolution processes of formic acid molecules on the ice films were more pronounced than desorption ($k_{ads}+k_{dis}\gg k_{des}$), within the timescale of our experiments. Therefore, although the high $N_s$ (uptake probability) values suggest a strong interaction between formic acid molecules and highly nitrated ice films, the $K_{Lin}$ and subsequently $\Delta H_{ads}$ and $\Delta S_{ads}$ values do not provide any significant information about the equilibrium between gas-phase and adsorbed formic acid molecules.

### 2.3. Atmospheric Implications

The atmospheric lifetime ($\tau$) of formic acid molecules due to heterogeneous loss on ice particles in cirrus clouds is given as $1/k_{het}$, within the kinetic limit, by assuming that the ice particles are in equilibrium and are not growing or evaporating. $k_{het}$ is the rate coefficient for the heterogeneous reaction and is given by Equation (15):

$$k_{het}=\frac{\gamma u A}{4} \qquad (15)$$

where $\gamma$ is the uptake coefficient, $u$ is the average molecular velocity, and $A$ is the surface area density of ice ranging between $2\times10^{-4}$ and $2\times10^{-7}$ $cm^2cm^{-3}$ for cirrus clouds.[47] Therefore, the atmospheric lifetime of formic acid can be determined as a function of temperature in the range 195–208 K, by using the $\gamma$ values determined in the present work, at two extreme cloud surface densities (see the Supporting Information, Figure S5). For pure ice surfaces and low $A$ values ($2\times10^{-7}$ $cm^{-1}$) the lifetimes are in the range 49–274 h, but since cirrus clouds do not last longer than 24 h, the removal of formic acid molecules by cirrus clouds is negligible. However, for high $A$ values
($2\times10^{-4}$ $cm^{-1}$) lifetimes are in the range 3–16 min; therefore, formic acid heterogeneous loss in dense cirrus clouds can be substantial and should be considered as a potent removal process for these molecules from the troposphere, in addition to their gas-phase photochemistry. Furthermore, for ice particles enriched with $HNO_3$, this removal process is independent of $HNO_3$ concentration, except for high $HNO_3$ concentrations (53.8 wt% $HNO_3/H_2O$) where the lifetime of formic acid molecules at 203 K is less than 1.5 h and 4 s for thin and dense cirrus clouds, respectively.

In addition, formic acid molecules may be removed from the atmosphere by their physical adsorption on cirrus cloud ice particles. In particular, $\alpha$ is defined by the expression [Eq. (16)]:

$$\alpha=\frac{[HCOOH]_{ads}}{[HCOOH]_g+[HCOOH]_{ads}}=\frac{K_{Lin}A}{1+(K_{Lin}A)} \qquad (16)$$

where $A$ is the surface area density and $K_{Lin}$ is the portion of formic acid molecules between the surface and the gas phase. The fractions, $\alpha$, are plotted as a function of surface area densities $A$ at 203 K, by using the $K_{Lin}$ values obtained at different ice surfaces, and are given in Figure 10. In dense cirrus clouds,

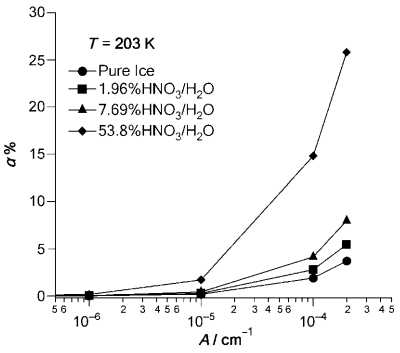


**Figure 10.** Fraction of formic acid molecules adsorbed on cirrus cloud ice particles versus surface area density $A$ ($cm^{-1}$) for pure ice particles and ice particles doped with $HNO_3$ at $T=203$ K.

a small fraction of formic acid molecules is removed to the condensed phase. On the contrary, at binary cirrus cloud particles ($HNO_3/H_2O$) the fraction of gaseous formic acid molecules accumulated on them becomes substantially high and reaches up to 25% for mixtures of 53.8 wt% $HNO_3$ in $H_2O$ clouds, due to dissolution of formic acid on a supercooled liquid layer.

## 3. Conclusions

Herein, we measured the initial uptake coefficient and adsorption uptakes of formic acid on thin ice films in the UT/LS temperature range. There was no evidence of formic acid dissociation on the polycrystalline ice films and the adsorption uptakes were reversible and exhibited Langmuir-type behaviour. Formic acid was bound on ice surfaces less strongly than strong acids HCl and $HNO_3$, OH radicals, $CH_3OH$, $CH_3C(O)CH_3$ and $N_2O_5$, with similar strength to HONO, and more strongly than $NO_3$, $NO_x$ and $O_3$. The adsorption enthalpy and entropy of formic acid on pure ice films were determined to be $\Delta H_{ads}=-(45.0\pm5.3)$ kJ $mol^{-1}$ and $\Delta S_{ads}=-(278\pm52)$ J $mol^{-1}K^{-1}$, based on the precursor adsorption model. The saturation surface coverage was determined to be $N_{max}=(2.94\pm0.67)\times10^{14}$ molecule $cm^{-2}$, and the temperature dependence of $K_{Lin}$ was derived as $K_{Lin}=(1.43\pm0.32)\times10^{-8}\exp[(4720\pm520)/T]$ $cm^3$ $molecule^{-1}$. The initial uptake coefficient and adsorption uptakes of formic acid on ice films doped with $HNO_3$ were found to increase substantially with increasing nitric acid concentration. The uptakes were enormous and irreversible at a high degree of nitration (53 wt%); this behaviour is consistent with the formation of a supercooled liquid layer that initiates

  

dissolution and probably diffusion processes. At low atmospheric temperatures, formic acid molecules will be scavenged by dense cirrus clouds very efficiently, and even more pronouncedly by cirrus clouds doped with $HNO_3$. Thus, heterogeneous loss of formic acid in the UT/LS could be a significant sink and substantially affect its atmospheric lifetime, in addition to gas-phase photochemistry.

## Acknowledgements

*This work was financially supported by a research grant from the Hellenic Ministry of Education under the program "PENED 2003", and the European Union by the project (SCOUT-O$_3$, EVK2-CT-1999-00005. This study was carried out in partial fulfilment of a doctoral dissertation (Dr. Manolis N. Romanias) at the Chemistry Department, University of Crete, Greece.*

**Keywords:** adsorption · atmospheric chemistry · formic acid · ice · thin films

[1] J. P. D. Abbatt, *Chem. Rev.* **2003**, *103*, 4783 – 4800, and references therein.
[2] J. H. Seinfeld, S. N. Pandis, *Atmospheric Chemistry and Physics*, Wiley, New York, **1998**.
[3] P. Khare, N. Kumar, K. M. Kumari, S. S. Srivastava, *Rev. Geophys.* **1999**, *37*, 227 – 248.
[4] W. L. Chameides, D. D. Davis, *Nature* **1983**, *304*, 427 – 429.
[5] A. Laaksonen, J. Hienola, M. Kulmala, F. Arnold, *Geophys. Res. Lett.* **1997**, *24*, 3009 – 3012.
[6] D. W. Fahey, R. S. Gao, K. S. Carslaw, J. Kettleborough, P. J. Popp, M. J. Northway, J. C. Holecek, S. C. Ciciora, R. J. McLaughlin, T. L. Thompson, R. H. Winkler, D. G. Baumgardner, B. Gandrud, P. O. Wennberg, S. Dhaniyala, K. McKinney, T. Peter, R. J. Salawitch, T. P. Bui, J. W. Elkins, C. R. Webster, E. L. Atlas, H. Jost, J. C. Wilson, R. L. Herman, A. Kleinbohl, M. von Konig, *Science* **2001**, *291*, 1026 – 1031.
[7] P. J. Popp, R. S. Gao, T. P. Marcy, D. W. Fahey, P. K. Hudson, T. L. Thompson, B. Karcher, B. A. Ridley, A. J. Weinheimer, D. J. Knapp, D. D. Montzka, D. Baumgardner, T. J. Garrett, E. M. Weinstock, J. B. Smith, D. S. Sayres, J. V. Pittman, S. Dhaniyala, T. P. Bui, M. J. Mahoney, *J. Geophys. Res. [Atmos.]* **2004**, *109*, D06302.
[8] A. K. Winkler, N. S. Holmes, J. N. Crowley, *Phys. Chem. Chem. Phys.* **2002**, *4*, 5270 – 5275.
[9] P. K. Hudson, M. A. Zondlo, M. A. Tolbert, *J. Phys. Chem. A* **2002**, *106*, 2882 – 2888.
[10] F. Dominé, L. Rey-Hanot, *Geophys. Res. Lett.* **2002**, *29*, 1873.
[11] N. Peybernès, C. Marchand, S. Le Calvé, P. Mirabel, *Phys. Chem. Chem. Phys.* **2004**, *6*, 1277 – 1284.
[12] P. von Hessberg, N. Pouvesle, A. K. Winkler, G. Schuster, J. N. Crowley, *Phys. Chem. Chem. Phys.* **2008**, *10*, 2345 – 2355.
[13] A. Symington, R. A. Cox, M. A. Fernandez, *Z. Phys. Chem. (München Ger.)* **2010**, *224*, 1219 – 1245.
[14] V. C. Papadimitriou, D. K. Papanastasiou, V. G. Stefanopoulos, A. M. Zaras, Y. G. Lazarou, P. Papagiannakopoulos, *J. Phys. Chem. A* **2007**, *111*, 11608 – 11617.
[15] K. G. Kambanis, Y. G. Lazarou, P. Papagiannakopoulos, *J. Chem. Soc. Faraday Trans.* **1996**, *92*, 3299 – 3303.
[16] J. Chao, B. J. Zwolinski, *J. Phys. Chem. Ref. Data* **1978**, *7*, 363 – 377.
[17] R. Büttner, G. Maurer, *Ber. Bunsen Ges.* **1983**, *87*, 877 – 882.
[18] A. Allouche, *J. Chem. Phys.* **2005**, *122*, 234703.
[19] S. Bahr, A. Borodin, O. Höfft, V. Kempter, *J. Chem. Phys.* **2005**, *122*, 234704.
[20] A. Borodin, O. Höfft, S. Bahr, V. Kempter, A. Allouche, *Nucl. Instrum. Methods Phys. Res. Sect. B* **2005**, *232*, 79 – 87.
[21] S. Hellebust, B. O'Riordan, J. Sodeau, *J. Chem. Phys.* **2007**, *126*, 084702.
[22] T. Huthwelker, M. Ammann, T. Peter, *Chem. Rev.* **2006**, *106*, 1375 – 1444.
[23] C. S. Boxe, B. R. Bodsgard, W. Smythe, M. T. Leu, *J. Colloid Interface Sci.* **2007**, *309*, 412 – 418.
[24] C. Manca, C. Martin, P. Roubin, *Chem. Phys.* **2004**, *300*, 53 – 62.
[25] C. Delval, M. J. Rossi, *J. Phys. Chem. A* **2005**, *109*, 7151 – 7165.
[26] X. Wei, P. B. Miranda, Y. R. Shen, *Phys. Rev. Lett.* **2001**, *86*, 1554 – 1557.
[27] M. T. Suter, P. U. Andersson, J. B. C. Pettersson, *J. Chem. Phys.* **2006**, *125*, 174704 – 174706.
[28] J. E. McDonald, *J. Geophys. Res.* **1965**, *70*, 1553 – 1554.
[29] D. M. Murphy, T. Koop, *Q. J. R. Meteorol. Soc.* **2005**, *131*, 1539 – 1565.
[30] J. Marti, K. Mauersberger, *Geophys. Res. Lett.* **1993**, *20*, 363 – 366.
[31] P. K. Hudson, J. E. Shilling, M. A. Tolbert, O. B. Toon, *J. Phys. Chem. A* **2002**, *106*, 9874 – 9882.
[32] R. G. Hynes, M. A. Fernandez, R. A. Cox, *J. Geophys. Res.* **2002**, *107*, 4797 – 4807.
[33] L. Chaix, H. van den Bergh, M. J. Rossi, *J. Phys. Chem. A* **1998**, *102*, 10300 – 10309.
[34] L. S. E. Romero Lejonthun, E. A. Svensson, P. U. Andersson, J. B. C. Pettersson, *J. Phys. Chem. C* **2009**, *113*, 7728 – 7734.
[35] K. D. Beyer, A. R. Hansen, *J. Phys. Chem. A* **2002**, 106, 10275 – 10284.
[36] D. R. Worsnop, L. E. Fox, M. S. Zahniser, S. C. Wofsy, *Science* **1993**, *259*, 71 – 74.
[37] L. F. Keyser, M. T. Leu, *Microsc. Res. Tech.* **1993**, *25*, 434 – 438.
[38] L. F. Keyser, M. T. Leu, *J. Colloid Interface Sci.* **1993**, *155*, 137 – 145.
[39] M. Boudart, G. Djega-Mariadassou, *Kinetics of Heterogeneous Catalytic Reactions*, Princeton University Press, Princeton, **1984**.
[40] J. T. Jayne, S. X. Duan, P. Davidovits, D. R. Worsnop, M. S. Zahniser, C. E. Colb, *J. Phys. Chem.* **1991**, *95*, 6329 – 6336.
[41] O. Sokolov, J. P. D. Abbatt, *J. Phys. Chem. A* **2002**, *106*, 775 – 782.
[42] NIST Standard Reference Database Number 69, http://webbook.nist.gov/chemistry/; NIST Chemistry WebBook, **2005**.
[43] M. Kerbrat, S. L. Calve, P. Mirabel, *J. Phys. Chem. A* **2007**, *111*, 925 – 931.
[44] M. Petitjean, P. Mirabel, S. L. Calvé, *J. Phys. Chem. A* **2009**, *113*, 5091 – 5098.
[45] T. Huthwelker, M. E. Malmström, F. Helleis, G. K. Moortgat, T. Peter, *J. Phys. Chem. A* **2004**, *108*, 6302 – 6318.
[46] J. P. D. Abbatt, *Geophys. Res. Lett.* **1997**, *24*, 1479 – 1482.
[47] S. Solomon, S. Borrmann, R. R. Garcia, R. Portmann, L. Thomason, L. R. Poole, D. Winker, M. P. McCormick, *J. Geophys. Res.* **1997**, *102*, 21411 – 21429.
[48] P. L. Cooper, J. P. D. Abbatt, *J. Phys. Chem.* **1996**, *100*, 2249 – 2254.
[49] R. G. Hynes, J. C. Mössinger, R. A. Cox, *Geophys. Res. Lett.* **2001**, *28*, 2827 – 2830.
[50] A. Aguzzi, M. J. Rossi, *Phys. Chem. Chem. Phys.* **2001**, *3*, 3707 – 3716.
[51] S. Seisel, B. Flückiger, M. J. Rossi, *Ber. Bunsen Ges.* **1998**, *102*, 811 – 820.
[52] P. Behr, A. Terziyski, R. Zellner, *J. Phys. Chem. A* **2006**, *110*, 8098 – 8107.
[53] F. F. Fenter, M. J. Rossi, *J. Phys. Chem.* **1996**, *100*, 13765 – 13775.
[54] L. Chu, G. Diao, L. T. Chu, *J. Phys. Chem. A* **2000**, *104*, 3150 – 3158.
[55] F. F. Fenter, M. J. Rossi, *J. Phys. Chem. A* **1997**, *101*, 4110 – 4113.
[56] O. W. Saastad, T. Ellermann, C. J. Nielsen, *Geophys. Res. Lett.* **1993**, *20*, 1191 – 1193.
[57] E. J. Dlugokencky, A. R. Ravishankara, *Geophys. Res. Lett.* **1992**, *19*, 41 – 44.

Received: May 30, 2010
Revised: August 31, 2010
Published online on October 19, 2010

  